Discrimination of DNA Hybridization Using Chemical Force Microscopy

Laura T. Mazzola,* Curtis W. Frank,*# Stephen P. A. Fodor,§ Curtis Mosher,¶ Raj Lartius,¶ and Eric Henderson¶

Departments of *Chemistry and #Chemical Engineering, Stanford University, Stanford, California 94305; §Affymetrix, Santa Clara, California 95051; and ¶Bioforce Laboratory, Ames, Iowa 50010 USA

ABSTRACT Atomic force microscopy (AFM) can be used to probe the mechanics of molecular recognition between surfaces. In the application known as "chemical force" microscopy (CFM), a chemically modified AFM tip probes a surface through chemical recognition. When modified with a biological ligand or receptor, the AFM tip can discriminate between its biological binding partner and other molecules on a heterogeneous substrate. The strength of the interaction between the modified tip and the substrate is governed by the molecular affinity. We have used CFM to probe the interactions between short segments of single-strand DNA (oligonucleotides). First, a latex microparticle was modified with the sequence 3′-CAGTTCTACGATGGCAAGTC and epoxied to a standard AFM cantilever. This DNA-modified probe was then used to scan substrates containing the complementary sequence 5′-GTCAAGATGCTACCGTTCAG. These substrates consisted of micron-scale, patterned arrays of one or more distinct oligonucleotides. A strong friction interaction was measured between the modified tip and both elements of surface-bound DNA. Complementary oligonucleotides exhibited a stronger friction than the noncomplementary sequences within the patterned array. The friction force correlated with the measured strength of adhesion (rupture force) for the tip- and array-bound oligonucleotides. This result is consistent with the formation of a greater number of hydrogen bonds for the complementary sequence, suggesting that the friction arises from a sequence-specific interaction (hybridization) of the tip and surface DNA.

INTRODUCTION

Atomic force microscopy (AFM) maps the topography of surfaces at molecular and atomic resolution (Binnig and Quate, 1986; Hansma et al., 1988; Albrecht et al., 1988). This technique has also proved useful in mapping molecular topography within biological systems (Hansma et al., 1997). AFM can also be used to probe the mechanical forces between surfaces, measuring friction force and adhesion between the AFM tip and sample (Mate et al., 1987; Burnham et al., 1990; Weisenhorn et al., 1992; Hoh et al., 1992; Overney et al., 1992; Wilbur et al., 1995).

At a microscopic level, the friction force depends on the molecular interactions of the two surfaces in sliding contact. These molecular forces can be further probed by manipulating the functionality of the AFM tip. For example, one can probe substrate functionality by varying the hydrophobicity of the AFM tip or by attaching a colloidal particle in place of the standard tip (Knapp et al., 1995; Ducker et al., 1991; Li et al., 1993; Rabinovich and Yoon, 1994). The tip can also be modified for specific chemical sensitivity. This technique has been dubbed "chemical force" microscopy (CFM), because the substrate can be mapped through chemical recognition between the surface and tip-bound functional groups (Nakagawa et al., 1993; Frisbie et al., 1994; Green et al., 1995; van der Vegte et al., 1997).

In a similar manner, biologically "active" AFM tips have been constructed to probe the interaction of proteins and ligands (Florin et al., 1994; Lee et al., 1994b), oligonucleotides (Lee et al., 1994a; Boland and Ratner, 1995), and other macromolecules (Dammer et al., 1995; Hinterdorfer et al., 1996). In these studies, the modified AFM tip was used to probe the specificity of biomolecular recognition by monitoring the force required to pull the modified tip away from its substrate in adhesion/rupture experiments.

The work presented here bridges the two approaches of chemical and biological recognition of CFM. We demonstrate a novel application of friction microscopy to characterization of the interaction of biological ligands, specifically short segments of DNA (oligonucleotides). This method provides a fast scan technique to differentiate the elements of a two-dimensional, heterogeneous substrate through molecular recognition. We have constructed patterned arrays of oligonucleotides that contain discrete, micron-scale elements in a checkerboard or stripe design (Pease et al., 1994). The arrays were then scanned with a DNA-modified AFM tip. As shown below, the elements of the substrate array could be differentiated by the friction force between the oligonucleotides of the tip and the substrate. However, the friction coefficient is sensitive to the molecular surface density as well as the mode of data acquisition and thus is not practical for quantifying molecular affinity. When a control (noncomplementary) oligonucleotide is included within a friction scan, the ratio of friction coefficients can be used as a reliable indicator of affinity. Finally, the friction force is shown to correlate with the adhesive force measured by adhesion/rupture experiments. By using the friction and adhesion methods in tan-

Received for publication 8 May 1998 and in final form 10 March 1999.

Address reprint requests to Dr. Curt Frank, Department of Chemical Engineering, Stanford University, Stanford, CA 94305-5025. Tel.: 650-723-4573; Fax: 650-723-9780; E-mail: curt@chemeng.stanford.edu

0006-3495/99/06/2922/12 $2.00

dem, CFM can be used for a fast analysis of affinity for multicomponent oligonucleotide arrays.

MATERIALS AND METHODS

Substrate preparation

The method for preparing oligonucleotide arrays has previously been described (Mazzola and Fodor, 1995; McGall et al., 1997). Briefly, glass wafers were cleaned in concentrated NaOH and rinsed exhaustively in water. The surface was derivatized for 2 h with a solution of 10% (v/v) mono(hydroxyethyl) aminopropyltriethoxysilane in 95% ethanol, rinsed, and dried in vacuo at 40°C.

In these experiments, a tetrathymidine linker was used for a flexible and hydrophilic boundary between the glass and the subsequent oligonucleotide probe. There is negligible cross-hybridization of tetrathymidine to the experimental probes, an improvement over the hexaethylene glycol linker used previously (Mazzola and Fodor, 1995). Using standard oligonucleotide synthesis protocols (Atkinson and Smith, 1984), we constructed the surface linker from three coupling cycles using 5′-dimethoxytrityl-2′-deoxythymidinephosphoramidite (DMT-dT-phosphoramidite) (ABI, Foster City, CA), followed by a cycle of 1-O′-(α-methyl-6-nitropiperonyloxycarbonyl)-hexaethyleneglycol-17-O-(*N,N*-diisopropylamino)-2′-deoxythymidinephosphoramidite (MeNPOC-dT-phosphoramidite). The custom MeNPOC protecting group is stable in a variety of solvents but can be removed by irradiation with 365-nm light.

The substrate was then selectively irradiated through a chrome-patterned lithographic mask (Photosciences, Torrence, CA). One mask contained patterns of 64-, 16-, and 4-μm checkerboard squares; another mask contained 5-μm stripes with a 15-μm spacing. In the simplest case, a single exposure was used to produce an activated surface pattern. An oligonucleotide was then constructed in the activated regions, using successive coupling cycles of DMT-phosphoramidites as described above to produce an array with alternating regions of oligonucleotide and base linker. If the first oligonucleotide was then capped, the entire surface could be irradiated to deprotect the remaining "background" sites for a second oligonucleotide synthesis in the newly activated sites. To construct the dual-probe substrates, the 5-μm stripes were activated first, followed by coupling to the 10-μm background regions. This process apparently resulted in a slightly greater density of surface molecules in the initially activated regions (vide infra), regardless of the order of oligonucleotide synthesis; however, this appeared to have no effect on the observed friction. The final site density of the surface oligonucleotides was $\sim 10^{16}$ molecules/m^2.

DNA probe selection

A 20-base DNA oligonucleotide was selected to investigate the sequence specificity of molecular recognition in our system. (The specificity and stability of DNA hybridization are easily controlled through the composition of the nucleotide bases (Breslauer et al., 1986). Hybridization is defined as the formation of duplex DNA through basepairing—the hydrogen-bonding of A/T and G/C bases of the single-strand partners. The number of contiguous matched pairs roughly defines the stability of a duplex.) The oligonucleotide 5′-CTGAACGGTAGCATCTTGAC forms a stable duplex with its complement at room temperature, with minimal interference due to self-complementarity or secondary structure (Forman et al., 1998); this sequence was immobilized to the AFM tip (see below). Three distinct oligonucleotide sequences were constructed on the substrate arrays. The 20-base sequence 3′-GACTTGCCATCGTAGAACTG (referred to as "the Complement") is the perfect match, or complement, to the tip-bound sequence and was present in all arrays. Two control probes were constructed to test the sequence specificity of hybridization: 3′-CAGTTCTACGATGGCAAGTC (Control A) and 3′-AGCTGACGAAATCTTCACAC (Control B). The two Control probes and the Complement have the same length and base composition, but only the Complement should hybridize to the tip-bound DNA. Control A is, in fact, the same sequence as presented on the modified tip and thus is not expected to self-hybridize with the tip-bound DNA. Control B is expected to have negligible affinity for any of the other oligonucleotide strands.

The array synthesis was confirmed independently by hybridization with presynthesized complementary oligonucleotides (Fig. 1). A dual-probe, 64-μm checkerboard array containing the Complement and Control A was sequentially incubated with a solution of the respective complementary oligonucleotides. Initially, the array was immersed in a 100 nM solution of the fluorescein-labeled tip-sequence oligonucleotide in 6× SSPE (1 M NaCl, 66 mM sodium phosphate, 6 mM EDTA, pH 7.4). After 1 h of incubation, the solution was replaced with fresh 6× SSPE to eliminate background fluorescence from the bulk solution and scanned by confocal fluorescence microscopy, using 488-nm excitation from an argon ion laser (3.4-μm beam resolution). As shown in Fig. 1 *A*, the tip-sequence oligonucleotide bound strongly to the regions on the array containing the Complement, with negligible hybridization to the regions containing Control A. Deionized water was then injected into the flow cell to remove the hybridized DNA. The array was then assayed under identical conditions with an oligonucleotide that binds to the Control A sequence. In Fig. 1 *B*, an inverse fluorescence pattern was obtained. The fluorescence intensities of the two images are similar (within 10%), suggesting a similar density of the synthesized probes. The same experiment was performed with a striped dual-probe array of the Complement and Control B, with comparable results (data not shown). The DNA arrays were stable when stored in the dark over a period of several weeks, as determined by reproduction of these fluorescence intensities.

Tip construction

DNA-functionalized AFM probes were constructed by bonding a DNA-derivatized microparticle to a silicon nitride AFM cantilever (BioForce Laboratory, Ames, IA). Specifically, an oligonucleotide with the sequence 5′-CTGAACGGTAGCATCTTGAC-NH_2-3′ was presynthesized with a conventional DNA synthesizer (Atkinson and Smith, 1984). A primary amine was positioned at the 3′ end, using Amino-Modifier C7 CPG starting material (Glenn Research, Sterling, VA). The amino-modified DNA was purified by gel electrophoresis and C18 column chromatography, as previously described (Henderson et al., 1987). The purified oligonucleotide was then coupled to COOH-functionalized, ~7-μm-diameter latex particles (Bang's Laboratories, Fishers, IN) by condensation in the presence of 1-ethyl-3(3-dimethylaminopropyl) carbodiimide (EDC) (Pierce, Rockford, IL). Approximately 100 μl of a 10% solids solution of microparticles was mixed with 1 ml of a solution containing 50 mM MES buffer (2-morpholinoethanesulfonic acid, pH 5.5) and 200 μg of 3′ amino-oligonucleotide. To this was added 100 μl of a 10 mg/ml EDC solution in ddH_2O. The solution was briefly vortexed and then incubated with gentle shaking for 2 h at room temperature. Particles were collected by centrifugation, washed twice by resuspension and centrifugation in 50 mM $NaPO_4$ (17 mM NaCl, pH 7.2), and then stored at 4°C in the wash buffer. The final density of

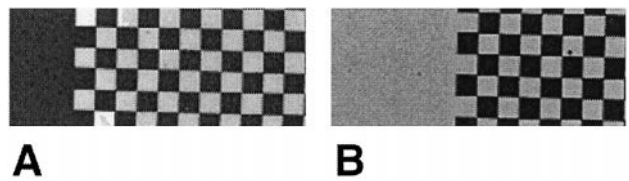

FIGURE 1 Confocal fluorescence image of a 64-μm checkerboard-patterned array of the Complement and Control A oligonucleotides. (*A*) Hybridized with a solution of fluorescein-labeled oligonucleotide that binds only to the Complement sequence. Fluorescence contrast is 540:45 counts (light:dark). (*B*) Hybridized with a solution of fluorescein-labeled oligonucleotide that binds only to the Control sequence. Fluorescence contrast is 530:30 counts.

probes is estimated from the initial parking area of the functional groups on the microparticle, ~50 Å^2/molecule, or ~10^6 molecules/μm^2.

For probe construction, a small aliquot of modified particles was briefly rinsed with ddH_2O, placed on a clean dry glass slide, and allowed to air dry. The particles were individually positioned with a micromanipulator (Narashige MN-4) at the ends of silicon nitride AFM probes (200 micron Nanoprobes; Digital Instruments, Santa Barbara, CA) and bonded into place with a quick-dry epoxy (Superglue Corp., Hollis, NY). Care was taken to buttress the particle against the preexisting pyramidal AFM tip and to avoid excessive use of epoxy that might occlude the contact surface. Once constructed, tips were used as soon as possible.

AFM imaging

AFM images were acquired using a Nanoscope III (Digital Instruments) with a 125 μm piezo scanner in contact mode. In this instrument, the sample is mounted on the piezo scanner and rastered beneath the tip. Laser light is deflected off the end of the cantilever onto a position-sensitive diode array detector. In this paper we refer to the orthogonal scans as "parallel" and "lateral" scanning modes. (These are referred to as height (0°) and friction (90°) modes in the DI software.) In parallel mode, the cantilever is rastered parallel to the long axis of the cantilever, and the deflection is detected using the detector as a two-part vertical array. In lateral mode, the cantilever is rastered orthogonally to the long axis of the cantilever, and deflection is detected using the detector as a two-part horizontal array.

Images were acquired using both the parallel and lateral scan directions with the feedback mechanism engaged. By this mechanism, the cantilever was maintained at a constant deflection by a feedback loop to the piezo mount. When the detector senses a change in deflection, the piezo servo adjusts the sample height to maintain the preset deflection of the cantilever. It should be noted that this is often referred to as "constant force" mode; however, this is not the case for materials that exhibit significant friction forces. As others have described (Warmack et al., 1994; Ruan and Bhushan, 1994), the cantilever is buckled and/or twisted when a strong lateral force is applied, even if the sample is topographically flat. For the parallel scans, this buckling can significantly change the position of the deflected laser beam on the detector. As shown in Fig. 2 (*right*), a buckling in the forward scan direction deflects the beam downward; the sample is then raised to retain the null position. The result is a greater pressure, or applied load, between the tip and sample than defined at the stationary position. When scanned in the reverse direction, the opposite effect is seen (Fig. 2, *left*). Thus the applied load is asymmetrical for the forward and reverse scans in the parallel mode. In our data, the observed parallel friction differed by 20% for the two directions; the averaged magnitude is presented. In the lateral scanning mode, friction produces a torsion distortion that has little effect on the piezo feedback mechanism. On average, the observed lateral friction differed by less than 5%. Friction data were quantified from the oscilloscope-mode friction "loops" rather than the image data to exclude any detector offset contribution to the data. These loops show the friction hysteresis of the forward and reverse scan directions, as the tip is repetitively traced over a single line. The detector output was calibrated to the cantilever deflection, using the static friction component of high-resolution friction loops (Liu et al., 1994). The calibration factors for the lateral and parallel scanning modes are $C_{LAT} = 4.7 \pm 0.7$ nm/V and $C_{PAR} = 26 \pm 14$ nm/V, respectively.

Surface topography was obtained using unmodified, sharpened silicon nitride tips with empirically minimized load. AFM and CFM data were acquired at 2 Hz. The 125 μm (J) scanner was calibrated for the *x*, *y*, and *z* axes twice within the experimental time period. Dry scans were performed at ambient conditions, typically 20–24°C and 30–35% humidity. Unless specified, solution images were obtained in 6× SSPE hybridization buffer (1 M NaCl), using the transparent AFM flow cell with ~200 μl capture-drop volume. Solutions were exchanged with a micropipette injector. To minimize evaporative effects, the solution data were acquired within 20 min of introduction.

The force-distance mode of the microscope was used to gauge the zero-value of the applied load as well as the rupture force between the applied tip and substrate. Data were acquired at a 0.1-Hz sampling rate. In addition, the vertical output of the detector was calibrated to the piezo movement by this method, or $C_{PIEZO} = 91 \pm 5$ nm/V. The normal spring constant for several standard and DNA-modified silicon nitride probes was measured from the thermal vibration frequency in air. All probes originated from the same wafer and had nearly identical spring constants ($k_N = 0.014 \pm 0.002$ N/m), indicating that the epoxied microparticle had little effect on the vertical flexibility of the cantilever.

RESULTS

AFM images of a 16-μm checkerboard oligonucleotide array are presented in Fig. 3. This array contains the 20-base Complement oligonucleotide, alternating with regions of the base tetrathymidine linker. The image in Fig. 3 *A* was obtained with a standard AFM tip in the parallel mode (reverse scan direction), in air, under ambient conditions. The topography of the oligonucleotide regions can be distinguished from that of the linker baseline, where the vertical dimension is represented by the hue of the color scale. The height difference between the two regions is ~15 Å and is attributed to the profile of the single-strand DNA. The same topography was detected using the tapping mode of the AFM (data not shown), which applies a significantly lower load force on surface structures, indicating that the AFM tip does not significantly compress the DNA (Yang et al., 1996). Stretched end to end, the extended oligonucleotide would measure ~140 Å (Saenger, 1988). The observed topography suggests that the surface is amorphous and that the flexible oligonucleotides have an isotropic orientation.

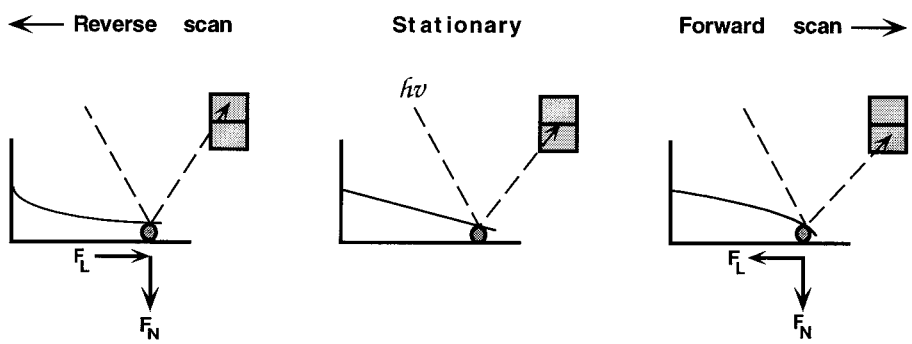

FIGURE 2 Illustration of cantilever buckling due to surface friction for scans parallel to the long cantilever axis. In the forward scan direction, friction deflects the laser beam downward (*right*). In the reverse direction, friction deflects the beam upward (*left*). Scan direction indicates cantilever motion relative to the surface.

FIGURE 3 Contact AFM scan of a 16-μm checkerboard-patterned DNA array containing the 20-base Complement oligonucleotide alternating with regions of the tetrathymidine base linker, acquired in height mode under ambient conditions. (*A*) Scanned with a standard silicon nitride tip, the image has a height contrast of ~15 Å. (*B*) Scanned with the DNA-modified tip, the image has an "apparent" height contrast of ~300 Å (note the change in scale).

The same DNA array was scanned under identical conditions in Fig. 3 *B*, now using the DNA-modified AFM tip. As before, the 16-μm checkerboard pattern is immediately apparent. However, the height scale of the image is now ~300 Å, 20 times greater than the height detected with an unmodified tip. This apparent increase in the height of the surface DNA is caused by a much stronger cantilever deflection across the alternating regions of the array. The increased deflection appears to be due to a strong frictional interaction between the DNA-modified tip and the surface. Surface topography could contribute a friction-like response, but this effect would be small and would appear only as a derivative component (Grafström et al., 1993). Surface compliance could also contribute to the observed contrast (Overney et al., 1994) and must be considered as these regions differ by 20 nucleotides, as must the possibility of chain entanglement of the DNA strands (Nakagawa et al., 1993). The friction contrast seen here is not simply the result of surface wetting (Fujihira et al., 1996) or differential surface charge (Hähner et al., 1997), as the entire surface is overlaid with the 4-base thymidine (T) linker. Furthermore, the contrast is due to more than just the outermost oligonucleotide bases (G versus T), as no contrast was observed for simple G/T or G/C arrays (data not shown). Instead, these images suggest that the contrast in Fig. 3 *B* arises from the molecular interaction of the tip and substrate oligonucleotides, which produces a detectable friction as the tip slides across the surface of the array. By the friction schematic of Fig. 2 (reverse scan direction), the bright regions should then correspond to regions of higher frictional force. Presumably, these regions contain the complementary DNA.

We then constructed an asymmetrical array for unambiguous identification of the surface-bound complementary DNA. In addition, we synthesized a second noncomplementary oligonucleotide in the alternating regions of the array to establish the sequence specificity of the molecular interaction. This dual-probe array contains regions of the Complement and Control B oligonucleotides; the regions have the same length and chemical composition but a different base arrangement of the DNA. The AFM images are now presented in units of the detector output (volts) rather than height to represent the friction magnitude. Unless specified, all subsequent images were acquired with the DNA-modified tips and scanned in the parallel mode.

Fig. 4 presents the forward (*A*) and reverse (*B*) images of a dual-probe array scanned with the modified tip immersed in deionized water (Complement = 10-μm stripes, Control = 5-μm stripes). Under these conditions, the complementary oligonucleotides should not hybridize, as the negatively charged structures repel each other in a neutral medium. As expected, there is little distinction between the complementary and control regions of DNA in either scan. The forward and reverse scans are practically identical; therefore the contrast is interpreted as real topography. (The observed 5-Å differential probably reflects a slight difference in surface density for the two oligonucleotide regions.) The topographical contribution is subtracted by taking the difference image (forward minus reverse) as shown in Fig. 4 *C*, which shows no discernible pattern within the baseline noise.

When hybridization buffer was introduced into the liquid cell, a marked increase in the surface contrast was observed. The lower half of Fig. 4 presents the forward (*D*) and reverse (*E*) scans of the array in the counterion-rich medium, presented at the same 250 mV scale. The contrast between the complementary and control regions of DNA is now ~100 mV. More significantly, the contrast in these images is also dependent on scan direction. In the forward scan direction, the complementary oligonucleotide regions appear darker than the control regions, indicating a stronger frictional response for the complementary DNA. In the reverse scan direction, the contrast is inverted, consistent with the schematic presented in Fig. 2. The friction contrast is effectively doubled in the difference image, Fig. 4 *F*.

The surface friction is affected by the concentration of counterions in the surrounding medium, as demonstrated in

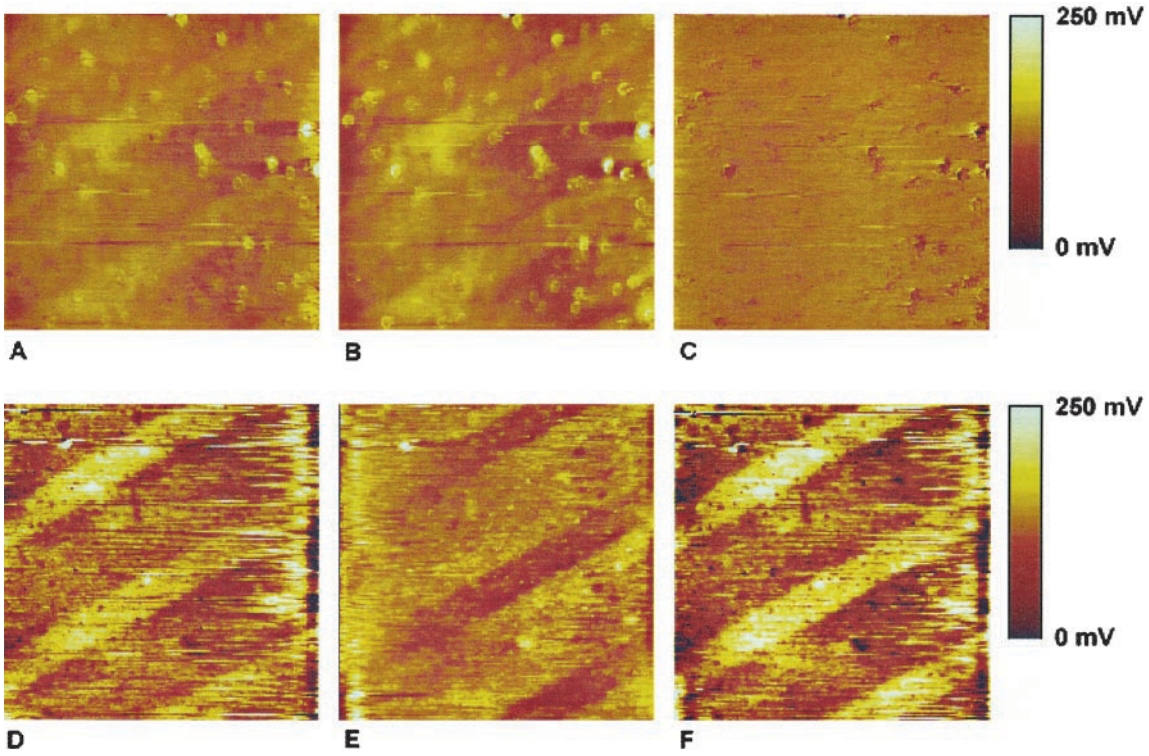

FIGURE 4 Contact AFM scan of a dual-probe array containing stripes of the Complement (10 μm) and Control (5 μm) oligonucleotides, scanned in deionized water with the DNA-modified tip. (*A*) Forward scan. (*B*) Reverse scan. (*C*) Difference image (forward minus reverse). The same array is scanned with the same tip in hybridization buffer. (*D*) Forward scan. (*E*) Reverse scan. (*F*) Difference image (forward minus reverse). The length scale is 50 μm and the vertical scale is 250 mV in all images.

the images in Fig. 5 *A–C*. As the salt concentration was increased from 1 to 2 M, the differential friction between the complementary and noncomplementary DNA regions also increased. The data are now presented only as difference images, in which the friction is approximately half the image contrast. The first image is identical to Fig. 4 *F*, now shown at a 700 mV scale, with a contrast of ~200 mV between the Complement and Control regions of DNA in 1 M NaCl (Fig. 5 *A*). In 1.5 M NaCl buffer, the contrast increased to ~270 mV (Fig. 5 *B*), and the 2.0 M NaCl buffer produced a ~700-mV differential (Fig. 5 *C*). This result is consistent with evidence that buffer concentrations up to 3 M NaCl effectively increase the rate of DNA nucleation (Orosz and Wetmur, 1977). The 3.5-fold enhancement in the friction contrast is comparable to the 2-fold rate increase observed for this concentration range. After the substrate was rinsed with deionized water, the friction faded within five "rinses" to resemble the data in Fig. 4 *C*, as expected for the reversible DNA interaction. Finally, the desalted DNA substrate was probed with a standard silicon nitride AFM tip to determine whether any topographical changes had occurred during the experiment. With the exception of

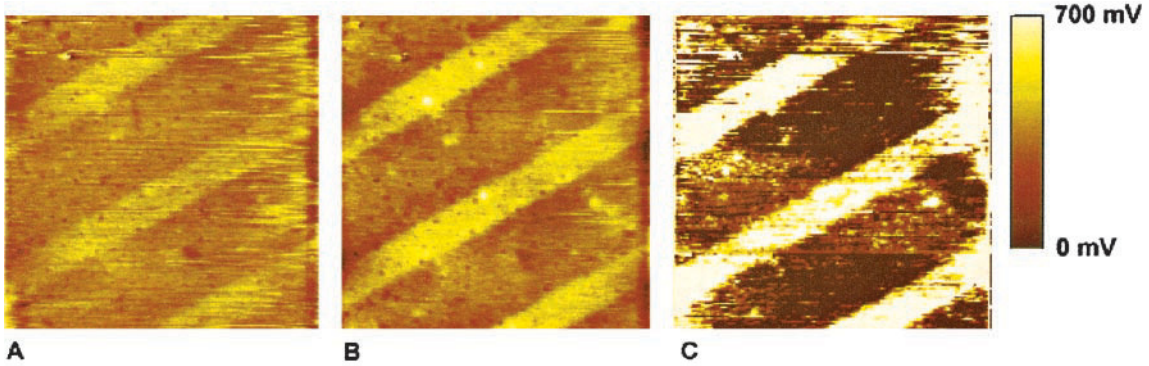

FIGURE 5 The friction differential between the Complement and Control regions increases with salt concentration. (*A*) Difference image in 1 M NaCl. (*B*) 1.5 M NaCl. (*C*) 2.0 M NaCl. The length scale is 50 μm and the vertical scale is 700 mV in all images.

precipitated salt, the overall topography appeared to be unchanged (data not shown).

The friction force also increases with the applied pressure (load) of the DNA-modified tip. As the tip is pressed into the substrate, the molecular contact area (and thus the friction) is increased by elastic deformation of the polystyrene support. In the experiment presented in Fig. 6, a line is repeatedly scanned across the surface of a dual-probe substrate in buffer (here, Complement = 5-μm stripes, Control = 10-μm stripes). The hysteresis between the forward and reverse lines reveals the magnitude of the friction at various loads. As seen in these images, there is measurable friction in both regions of the DNA substrate, but the magnitude is consistently larger for the complementary DNA. When the friction (half the total hysteresis) is plotted versus the applied load, the data can be fit to a simple linear function. Data are presented in Fig. 7 for both the lateral and parallel scanning modes acquired in a single experiment. A direct comparison of the two modes requires a sophisticated response analysis (see Appendix). Nevertheless, the relative friction response of the complementary and noncomplementary DNA yields useful information. For both the parallel and lateral modes of acquisition, the slope of the complementary data is 1.5 times greater than the slope of the noncomplementary data. This ratio is equal to the ratio of friction coefficients, and it indicates the relative friction response of the complementary versus control DNA interactions. This "normalized" friction parameter may be used to compare the strength of molecular affinity in this system.

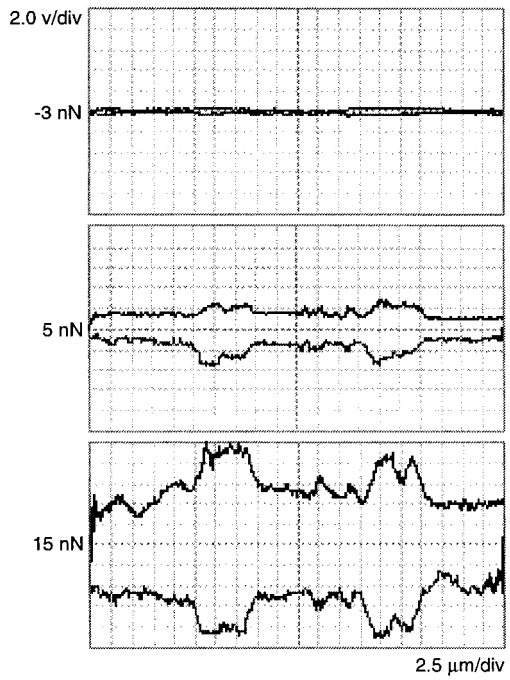

FIGURE 6 Friction "loops" demonstrating the friction hysteresis with increasing applied load. Here the modified tip is scanned back and forth in a line across a substrate containing regions of complementary (*thin stripes*) and noncomplementary (*thick stripes*) oligonucleotides. The friction force is half the observed hysteresis.

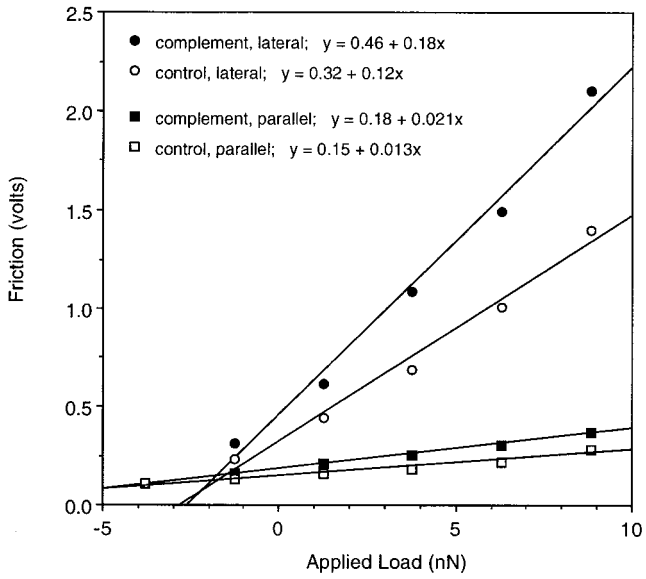

FIGURE 7 Friction signal versus applied load for the parallel and lateral scanning modes, acquired in a single experiment. The ratio of slopes (complement/control) is ~1.5 for both parallel and lateral modes.

In all data of Fig. 7, there is a detectable friction at zero applied load, evidence of a strong adhesive component that contributes to the frictional interaction. At the adhesion limit, a contact-rupture force can be extrapolated from the data as the observed friction approaches zero. The data in Fig. 7 give a rupture force of ~3 nN for the lateral mode and ~10 nN for the parallel mode. (One would expect that the adhesive load would be greater for the complementary DNA in each case; this could be resolved with a greater number of data points near the adhesion limit.) The lateral and parallel data were acquired within the same experiment, yet the parallel mode consistently gave a larger rupture force than the lateral mode. This was observed regardless of the order of data acquisition, even when the data points were interleaved, suggesting that there is a significant difference in the surface contact for the two modes near the adhesion limit.

Friction data were acquired from different batches of modified tips. We observed that both the adhesive load and slope of the friction varied within a factor of 3, depending on the tip used in each experiment. This is probably due to variation in the oligonucleotide surface density of each synthesis, coupled with the individual microparticle size and contour. The friction coefficient is known to decrease for high-density polymer surfaces (Bely et al., 1982). A high density generally induces a greater cohesion between surface molecules, thus lowering the accessibility for intercalating strands. It can also reduce the overall elasticity of the surface, which lowers the contact area for a given normal load. Indeed, we observed that the frictional response decreased as the microparticle coupling reaction was pushed toward saturation, as shown in Fig. 8. However, the slope ratio (1.3) is essentially the same as for the lower-density DNA tips. The high-density tips also required a stronger

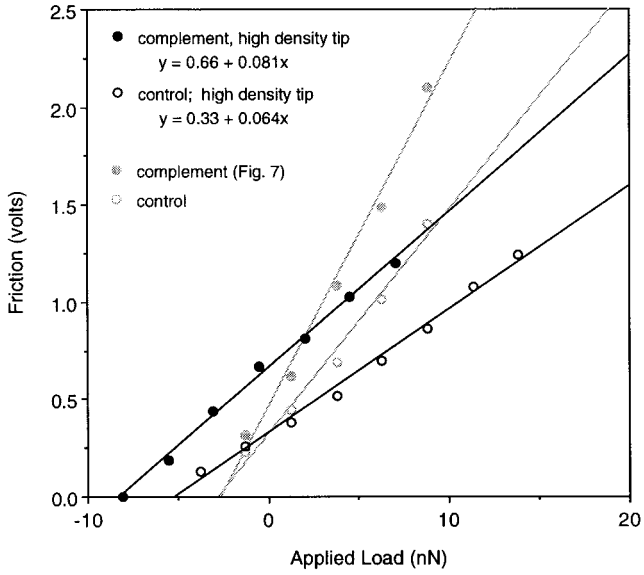

FIGURE 8 Friction signal versus applied load for the high-density modified tips. The friction response (slope) decreases with increasing density of the tip-bound DNA. The friction response for the "moderate" density tips of Fig. 7 is shown in gray.

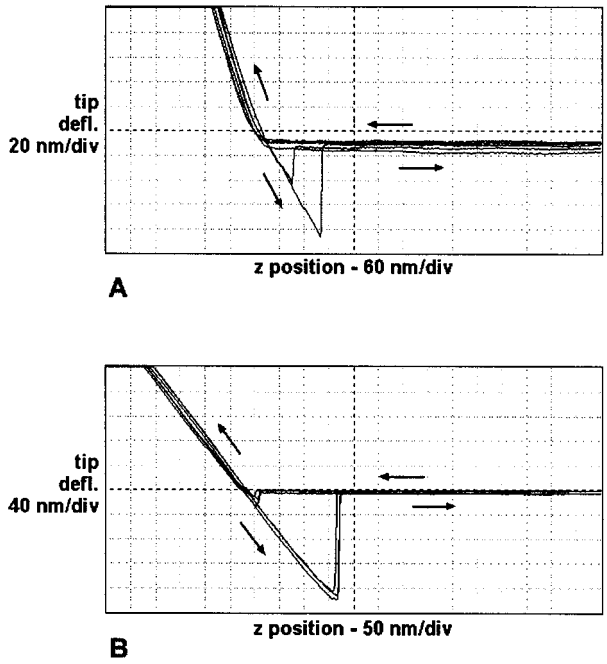

FIGURE 9 Rupture curves for the high-density DNA tips applied to the (*A*) Control and (*B*) Complement DNA arrays. The rupture force for the control data varied randomly between 0 and 2 nN (1.2 nN weighted average). The rupture force for the complementary data was consistently 2.7 nN.

rupture force at the adhesion limit, where the energies of the two interfaces were now clearly distinct. The complementary regions required 8.3 nN of rupture force, compared to the 5.2 nN required for the noncomplementary regions.

Finally, the adhesion between the modified tips and the substrate DNA was sampled directly by using the force-distance application of the AFM. In this application, a modified tip was applied to the substrate and then pulled from contact. The force required to separate the surfaces is mapped by the rupture curves of Fig. 9. To clarify the molecular species, this experiment was carried out on individual substrates of the Complement and Control DNA rather than the dual-probe array, using the same tip as in Fig. 8. Rupture curves for the noncomplementary DNA substrate are presented in Fig. 9 *A*. These data fell into roughly three categories: for the >30 adhesion curves obtained with this sample, 8% produced zero adhesion, 58% produced a ~0.8 nN rupture force, and 34% produced a ~2 nN rupture force. The variance in the rupture force does not suggest damage to the substrate or tip, as they were randomly distributed throughout the sampling interval. In contrast, the subsequent rupture curves for the complementary DNA substrate had a highly reproducible rupture force of 2.7 nN, as shown in Fig. 9 *B*. These curves also exhibit a large "jump-to-contact" as the tip nears the complementary surface. A similar effect was seen in the adhesion measurements of nucleotide-coated gold surfaces, which was attributed to long-range electrostatic forces (Boland and Ratner, 1995). In our data, this attraction appears to arise from a sequence-specific affinity of the complementary strands, as the attractive force (~0.3 nN) is absent in the noncomplementary data.

DISCUSSION

We have demonstrated how a DNA-functionalized tip can differentiate the surface-bound elements of a DNA array through both friction and adhesion. A stronger friction force was detected for the complementary DNA substrate compared to the noncomplementary regions. Furthermore, the source of the friction appears to be characteristic of a hydrogen-bond interaction. This result parallels the observed surface adhesion, strongly suggesting that discrimination occurs via a sequence-specific molecular recognition (hybridization) of the DNA strands. The magnitude of the surface force and energy of this system can be calculated by simple mechanical analysis of the normal and lateral forces.

Hybridization

The DNA adhesion observed in these experiments is probably only a partial hybridization of the tip and substrate DNA, because of the limited time of contact between the surfaces. Although the rate constant for array hybridization is the same as observed in solution ($k_{on} \approx 10^5\ M^{-1}\ s^{-1}$), it has been shown that the binding mechanism does not immediately lead to the fully duplexed structure (Forman et al., 1998). Strands of DNA initially bind to more than one surface molecule, forming a "bridge" between neighboring sites. Complete hybridization is reached only after a slow reorganization (>2 h) of the surface-bound strands. Nevertheless, the partially bound state is still informative, because

the entire sequence is represented within the sum of partial or "bridged" hybrids. This collective interaction can be used to map oligonucleotide sequences at single basepair discrimination (Pease et al., 1994; Wang et al., 1998).

Our data show that sequence recognition also occurs when DNA is bound to the modified tips. In this case, the interaction is constrained by the transient contact of the tip and substrate. The fast scan rate (200 μm/s) acutely limits the hybridization at the DNA interface. The surface interaction should then reflect the energy of partial hybridization rather than the fully duplexed DNA, which might account for the similarity in signal for the complementary and noncomplementary strands. The friction of the noncomplementary strands represents the baseline signal for our system (random basepairing, van der Waals and electrostatic forces). The sensitivity, or ratio of Complement to Control, indicates the dynamic range. Our 1.5-fold range in signal is conspicuously low compared to the solution hybridization of Fig. 1, in which the signal ratio is closer to 20. This difference is undoubtedly due to the distinct time scales for hybridization. Increasing the time of contact between the modified tip and sample should greatly enhance the dynamic range of our system. By this method, it should be possible to monitor the transition to the fully duplexed DNA. This approach would allow a more accurate measure of the duplex energy and consequently increase the sensitivity of this technique.

Friction

The friction demonstrated here arises from a complex molecular interaction, but the force can still be evaluated by classical mechanical analysis (Pollock, 1992). Friction is characterized by deformation and adhesion of the interface, which are generally believed to act independently. In the case of molecularly smooth surfaces, friction is primarily a function of adhesion and is therefore proportional to the contact area of the interface. The contact is controlled through the pressure, or load, of the system. The friction force can be defined as $F = \mu L_{\text{total}}$, where μ is the friction coefficient and L_{total} is the sum of the external load (applied) and the internal load of adhesion, or $F = \mu(L_{\text{ext}} + L_{\text{int}})$.

The friction coefficient describes the friction response of the interface during sliding contact. It is not a true parameter of the molecular interface, however, as it is sensitive to a number of experimental parameters. (Only the coefficients obtained under identical conditions can be quantitatively compared.) As shown earlier, the friction coefficient is sensitive to surface density. Friction coefficients can also be modulated by the applied load or scan rate of the tip. The friction in our experiments was linear over a 10-fold range in applied load and a 4-fold range of scan rates, indicating that the friction coefficient was fairly insensitive within these parameters. In our case, it is likely that the load is too low and the scan rates too high to greatly affect the friction coefficient. As described above, it should be possible to increase the friction response by scanning at a much slower rate. A practical scan limit would depend on the duration and stability of the scan, which would be defined by the size of the substrate matrix. The data presented here suggest that friction microscopy may be most useful as a fast but low-resolution technique to differentiate the species within a multicomponent array.

Lateral friction signal

To determine the magnitude of the observed friction signal (F), the detector output must first be calibrated to the physical deflection of the cantilever (C), and then multiplied by the appropriate spring constant (k):

$$F(\text{N}) = F(\text{volts}) * C * k$$

For the lateral scan direction, the spring constant of torsional deflection (k_{LAT}) can be calculated by modeling the torsional deflection of the triangular cantilever (Neumeister and Ducker, 1994; Noy et al., 1995). This equation can be empirically derived by using the normal spring constant to obtain $k_{\text{LAT}} = 6.0$ N/m. Combined with the lateral calibration factor, the friction equation reduces to $F_{\text{LAT}}(N) = F_{\text{LAT}}(V) * 28$ nN/V. The calibrated data of Fig. 8 are plotted in Fig. 10.

For the calibrated data, friction coefficients of ~5 and 3 are extracted from the slopes of the Complement and Control data, respectively. The magnitude of these coefficients is unusually large. Friction coefficients typically range between 0.01 and 2.0, where "low" friction coefficients are $\leq$0.3 and "high" friction coefficients are $\geq$1.0 (Singer, 1992). Friction coefficients of polymers generally range between 0.01 and 0.5, where the strongest friction occurs

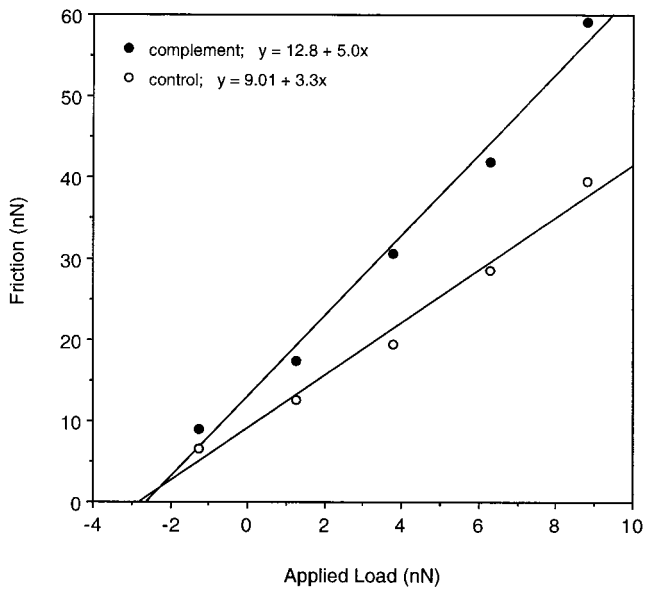

FIGURE 10 Friction force for the lateral scanning mode. Friction coefficients are ~5 and 3 for the Complement and Control DNA, respectively.

with flexible, long-chain polymers (Bely et al., 1982). Friction coefficients of 0.03–2.5 have been measured for chemically functionalized surfaces, where the strongest friction occurs with carboxylic acid-terminated monolayers (Noy et al., 1997). These trends show that hydrogen-bonding functional groups produce the strongest friction, and that friction is enhanced by polymer entanglement (which increases the molecular overlap). Because DNA is specially designed for entangled H-bond interactions, it is reasonable that the friction coefficients would be large, as seen here.

Adhesion

The adhesive strength of the DNA interface is sampled directly by the adhesion measurements and indirectly by the friction force. In both cases, the adhesion is detected by the contact-rupture force required to separate the two surfaces. The two methods are not identical, as the friction has an additional tangential component to the force (Savkoor, 1992), but the magnitudes of the rupture force should be similar. The data for the high-density DNA tips show this to be true: for the complementary DNA, the 8.3-nN rupture load of friction is comparable to the 2.7-nN rupture force of adhesion. For the noncomplementary DNA, the 5.1-nN rupture load can be compared to the largest rupture force of adhesion (2 nN) or the 1.2-nN weighted average. The sensitivity is equivalent for the two methods (1.6 versus 1.4) for the sampling conditions presented here. Unlike the friction experiments, however, the sensitivity of the adhesion measurements could be easily enhanced by increasing the tip-contact time before rupture. (Variation of the tip-contact time was not available with the software used for our data acquisition. Recent software versions now include this option.) Slow rates of surface adhesion have been demonstrated with similar systems of immobilized DNA (Florin et al., 1995), protein (Stuart and Hlady, 1995), and polymers (Chen et al., 1991), suggesting that surface reorganization plays a key role in the adhesion of complex molecular interfaces.

Others have shown that the mechanics of the AFM tip interaction are well described by the JKR theory of adhesion (Noy et al., 1995; van der Vegte and Hadziioannou, 1997), in which the elastic deformation of a sphere at a rigid surface is attributed to external and internal forces (Johnson et al., 1971; Israelachvili, 1992). This model predicts that the rupture force of the interface (F_R) depends simply on the size of the sphere (radius R) and the work of adhesion (W):

$$F_R = -(3/2)\pi RW$$

For the 2.7-nN rupture force required to separate the complementary DNA interface, we calculate 1.6×10^{-4} J/m^2 for the work of adhesion. The sequence-specific contribution to the adhesion can be obtained by comparing the adhesion of the complementary versus noncomplementary interfaces. Thus the difference in rupture force can be used to estimate the energy of the basepair hydrogen bonds, or $\sim 1 \times 10^{-4}$ J/m^2. Using the molecular packing density of the DNA arrays, this work corresponds to a molecular bond energy of ~2 kcal/mol. The magnitude of this interaction is comparable to the strength of most hydrogen bonds (Thomas et al., 1995; Hoh et al., 1992) but it is much smaller than the 40 kcal/mol free energy or the 140 kcal/mol enthalpy predicted for the complementary duplex (Breslauer et al., 1986). (The rupture force for biomolecular adhesion has been shown to correlate with the enthalpy rather than the free energy of adhesion (Chilkoti et al., 1995).) A low surface energy could be explained if 1) not all of the surface molecules interact, or 2) only a few hydrogen bonds form per molecule. It could be the case that only 5% of the surface molecules are available for hybridization, as was concluded in adhesion measurements of Colton and coworkers (Lee et al., 1994a). However, their surface accessibility was constrained by a self-complementary oligonucleotide sequence—not an issue in our case. We suggest instead that the surface energy is low because the DNA is not at equilibrium, or full duplexation, before rupture of the interface. This model is consistent with the kinetic analysis of the friction data presented above.

The JKR theory also predicts that the contact area of the interface (radius a) is a function of the elasticity ($K = 3.4 \times 10^9$ J/m^3 for polystyrene) and the total load:

$$a^3 = (R/K) * (L_{ext} + L_{int})$$

where

$$L_{int} = 3\pi RW + [6\pi RWL_{ext} + (3\pi RW)^2]^{1/2}$$

Given the work of adhesion calculated above, interfacial rupture should occur at ~500 nm^2, corresponding to roughly five molecules on the DNA array. One could then estimate an average rupture force of ~0.3 nN per molecule for the hydrogen-bond component of the complementary DNA. The adhesion work of Boland and Ratner with nucleotide monolayers suggests that DNA basepairs correspond to an average ~54-pN rupture force (Boland and Ratner, 1995). One could conclude from their data that our rupture force corresponds to the bonding of ~5 bp per molecule. The strength of such an interaction is consistent with the bond energy calculated above.

Stability

The data presented here showed no direct evidence for mechanical damage to the tip or substrate as a result of the repeated friction or rupture analyses. The signals were highly reproducible, even after 4 h of continuous scanning. The data showed no sudden loss of signal that might indicate probe "shedding" from the tip or substrate, which is consistent with a bond energy well below the magnitude for covalent interactions. For our system, it is reasonable to assume that any friction-generated heat is quickly dissipated by the surrounding liquid medium. Slight changes in the local temperature could destabilize the DNA hybridization,

which would further depress the observed binding energy. Although it is likely that some mechanical damage or deformation does occur over time, the friction and rupture force experiments proved to be surprisingly robust.

Interestingly, the data in Fig. 3 present an apparent exception to the rule that hybridization can only take place in an counterion-rich medium. In Fig. 3 *B*, the DNA array was scanned in air using the DNA-modified tip. Under these conditions, only a hydration layer of water should be present at the surface, and the DNA interaction should be repulsive across the entire array (Butt, 1991). The electrostatic repulsion of unshielded DNA is demonstrated by the data of Fig. 4, where no hybridization (friction) was observed in a medium of deionized water. Clearly, though, the tip in Fig. 3 *B* shows a strong attraction to the complementary regions of the substrate. An explanation may be found by considering the ionic strength of the hydration layer. Although the surfaces in Fig. 3 were rinsed in deionized water, the water may have contained residual ions at extremely low concentration. As the surfaces were quickly dried, dehydration would concentrate this residue at the surface. In this case, the thin film of the hydration layer could have an ionic strength that would differ significantly from that of bulk water. If real, the charged layer would alleviate some of the electrostatic repulsion of the negatively charged DNA. The observation of DNA basepairing under ambient conditions is of considerable value to the practical application of this technique, permitting a fast and easy measure of the components within the matrix. By including a standard sequence within each array, individual scans could be normalized and compared for a variety of scanning conditions.

CONCLUSIONS

We have used chemical force microscopy to probe the mechanics of molecular recognition on a two-dimensional biomolecule array. We have shown how surface-bound oligonucleotides can be differentiated by both friction and adhesion force. The sensitivity of these techniques is constrained by the time scale for binding and surface reorganization. These methods appear to work best in tandem, where the friction force can first be used to quickly differentiate the array elements, followed by a more sensitive probe of the energies by the adhesion/rupture force. This combination of techniques could be used to calibrate the surface energy of DNA hybridization to the molecular composition. For example, the length and base arrangement of the immobilized DNA can be systematically varied within an array. A single friction/adhesion experiment would reveal the molecular adhesion energy. Of particular interest would be the effect of incorporating mismatch (noncomplementary) bases within an otherwise complementary structure. With a concurrent improvement in signal to noise, it may be possible to use this technique to calibrate single-basepair hybridization energies.

As a final observation, the tensile strength (F_R/m^2) of the complementary DNA interface shown here was $\sim 5 \times 10^6$ N/m^2. If the hybridization approached equilibrium, one would expect this factor to increase by at least an order of magnitude, putting the DNA interface on par with the strength of common adhesives (10^6-10^8 N/m^2; Perry, 1984). Most compelling is the fact that the DNA adhesion is completely reversible under controlled conditions. This feature may have great potential for the development of biomedical devices, where a strongly bonding biocompatible interface is crucial.

APPENDIX: PARALLEL FRICTION SIGNAL

The method of Neumeister and Ducker method can be used to calculate a parallel spring constant of $k_{PAR} = 7.4$ N/m, which combines both bending and buckling modes of cantilever deflection for the parallel mode of scanning. One might then assume that the friction reduces to $F_{PAR}(N) = F_{PAR}(v) * C_{PAR} * k_{PAR}$, which should equal the friction obtained in the lateral mode for an isotropic tip interaction. However, these data require a more careful interpretation, as there is an obvious difference between the parallel friction and lateral friction at low load—most noticeably the ~7-nN difference in load at the adhesion limit. We believe that this difference arises from the servo-feedback response, which augments the externally applied load. The applied load becomes $L'_{ext} = L_{ext} + L_s$ for the parallel mode. The servo contribution (L_s) would be more conspicuous when the external load is small. Warmack and co-workers observed a similar servo-enhanced friction at low load for parallel-mode scanning (Warmack et al., 1994). They demonstrated how the friction could be accurately fit by the inclusion of a servo force at low load. In our case, the servo force can be estimated by a simple calibration of the parallel and lateral data of Fig. 7.

For this calibration, we assume that there is no servo response for the lateral mode imaging. A comparison of the parallel and lateral data should then reveal the servo-induced component of the parallel mode. This effect is clearly shown by the ratio of the raw data, $F_{PAR}(V)/F_{LAT}(V)$ in Fig. 11 *A* (*inset*). This ratio would be constant if the lateral and parallel modes were equivalent. Instead, the ratio is large near the adhesion limit but asymptotically approaches a constant value (~0.17) for loads greater than 10 nN. (The averaged data were fit to an exponential decay: $y = 0.168 + 0.37\exp\{-(x + 1.26)/3.46\}$, where $y = F_P(V)/F_L(V)$ and $x = L_{ext} * 10^9$.) Past the 10 nN limit, the signal appears to be equivalent for parallel and lateral detection. Making the assumption that the friction response is equivalent, $F_{LAT}(N) = F_{PAR}(N)$, then

$$k_{PAR}/k_{LAT} = [F_{LAT}(V)/F_{PAR}(V)] * [C_{LAT}/C_{PAR}]$$
$$= 1.06 \text{ for loads} > 10 \text{ nN}$$

Thus one would extract a parallel spring constant, $k_{PAR} \approx 6.4$ N/m, very close to the theoretical value. This result suggests that the two modes are indeed equivalent for loads greater than 10 nN. To accurately compare the friction below that limit, one would have to adjust the parallel load to include the servo-induced force. Using the fit to the ratio data above:

$$F_{PAR}(N)/F_{LAT}(N) = \left(\frac{C_{PAR} * k_{PAR}}{C_{LAT} * k_{LAT}}\right) * y$$

Because $F_{LAT}(N) = \mu(L_{ext} + L_{int})$ and $F_{PAR}(N) = \mu(L'_{ext} + L_{int})$, this equation reduces to

$$L_s = \{5.9 * y - 1\} * (L_{ext} + L_{int})$$

Although the adhesive load L_{int} varies with the external load (vide infra), the servo force can be closely approximated by using $L_{int} = 3$ nN for the limited range applied here. (The servo force will be slightly underestimated at higher loads.) The components L_s and L_{ext}' are plotted versus L_{ext} in Fig. 11 *A*. Whereas the applied load ranges between −10 and 10 nN, the actual

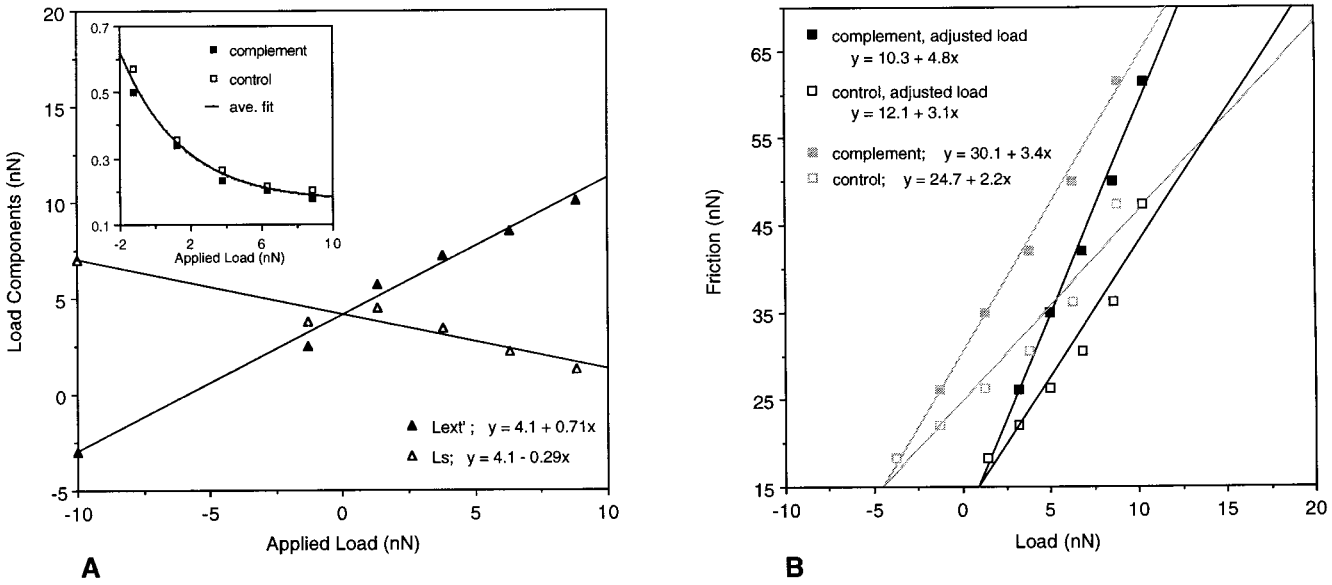

FIGURE 11 Calibration of the parallel and lateral scanning modes. (*A*) Servo-force contribution to the applied load (L_s) and the total external load ($L'_{ext} = L_{ext} + L_s$) and the friction response of the parallel versus lateral mode (*inset*). (*B*) Friction force for the parallel scanning mode using the calibrated load, L'_{ext}. The friction force for the uncalibrated load is shown in gray.

load at the sample ranges between −3 and 10 nN because of the contribution of the servo force. The parallel friction is then plotted as a function of both L_{ext} and L_{ext}' in Fig. 11 *B*, to illustrate the effect of the adjustment on the friction coefficient.

We thank E. Gentalen for his instruction in fabricating the DNA arrays, Dr. T. Middendorf for many helpful discussions, and our reviewers for their helpful comments.

This work was supported in part by the National Institutes of Health–Stanford Biotechnology Training grant and the Center on Polymer Interfaces and Macromolecular Assemblies (CPIMA), through the NSF-MRSEC program, DMR 94-00354.

REFERENCES

Albrecht, T. R., M. M. Dovek, C. A. Lang, P. Grütter, C. F. Quate, S. W. J. Kuan, C. W. Frank, and R. F. W. Pease. 1988. Imaging and modification of polymers by scanning tunneling and atomic force microscopy. *J. Appl. Phys.* 64:1178–1184.

Atkinson, T., and M. Smith. 1984. Solid phase synthesis of oligodeoxyribonucleotides by the phosphite-triester method. *In* Oligonucleotide Synthesis: A Practical Approach. M. J. Gait, editor. IRL Press, Oxford, England. 35–81.

Bely, V. A., A. I. Sviridenok, M. I. Petrokovets, and V. G. Savkin. 1982. Structure and frictional properties. *In* Friction and Wear in Polymer-Based Materials. Pergamon Press, Oxford. 187–193.

Binnig, G., and C. F. Quate. 1986. Atomic force microscope. *Phys. Rev. Lett.* 56:930–933.

Boland, T., and B. D. Ratner. 1995. Direct measurement of hydrogen bonding in DNA nucleotide bases by atomic force microscopy. *Proc. Natl. Acad. Sci. USA.* 92:5297–5301.

Breslauer, K. J., R. Frank, H. Blöcker, and L. A. Marky. 1986. Predicting DNA duplex stability from the base sequence. *Proc. Natl. Acad. Sci. USA.* 83:3746–3750.

Burnham, N. A., D. D. Dominguez, R. L. Mowery, and R. J. Colton. 1990. Probing the surface forces of monolayer films with an atomic force microscope. *Phys. Rev. Lett.* 64:1931–1934.

Butt, H.-J. 1991. Electrostatic interaction in atomic force microscopy. *Biophys. J.* 60:777–785.

Chen, Y. L., C. A. Helm, and J. N. Israelachvili. 1991. Molecular mechanisms associated with adhesion and contact angle hysteresis of monolayer surfaces. *J. Phys. Chem.* 95:10736–10747.

Chilkoti, A., T. Boland, B. D. Ratner, and P. S. Stayton. 1995. The relationship between ligand-binding thermodynamics and protein-ligand interaction forces measured by atomic force microscopy. *Biophys. J.* 69:2125–2130.

Dammer, U., O. Popescu, P. Wagner, D. Anselmetti, H.-J. Güntherodt, and G. N. Misevic. 1995. Binding strength between cell adhesion proteoglycans measured by atomic force microscopy. *Science.* 267:1173–1175.

Ducker, W. A., T. J. Senden, and R. M. Pashley. 1991. Direct measurement of colloidal forces using an atomic force microscope. *Nature.* 353: 239–241.

Florin, E.-L., V. T. Moy, and H. E. Gaub. 1994. Adhesion forces between individual ligand-receptor pairs. *Science.* 264:415–417.

Florin, E.-L., M. Rief, H. Lehmann, M. Ludwig, C. Dornmair, V. Moy, and H. E. Gaub. 1995. Sensing specific molecular interactions with the atomic force microscope. *Biosens. Bioelectron.* 10:895–901.

Fodor, S. P. A., J. L. Read, M. C. Pirrung, L. Stryer, A. T. Lu, and D. Solas. 1991. Light-directed, spatially addressable parallel chemical synthesis. *Science.* 251:767–773.

Forman, J. E., I. D. Walton, D. Stern, R. P. Rava, and M. O. Trulson. 1998. Thermodynamics of duplex formation and mismatch discrimination on photolithographically synthesized oligonucleotide arrays. *In* Molecular Modeling of Nucleic Acids, ACS Symposium Series 682. 206–228.

Frisbie, C. D., L. F. Rozsnyai, A. Noy, M. S. Wrighton, and C. M. Lieber. 1994. Functional group imaging by chemical force microscopy. *Science.* 265:2071–2074.

Fujihira, M., D. Aoki, Y. Okabe, H. Takano, H. Hokari, J. Frommer, Y. Nagatani, and F. Sakai. 1996. Effect of capillary force on friction force microscopy: a scanning hydrophilicity microscope. *Chem. Lett.* 7:499–500.

Grafström, S., M. Neitzert, T. Hagen, J. Ackermann, R. Neumann, O. Probst, and M. Wörtge. 1993. The role of topography and friction for the image contrast in lateral force microscopy. *Nanotechnology.* 4:143–151.

Green, J.-B. D., M. T. McDermott, M. D. Porter, and L. M. Siperko. 1995. Nanometer-scale mapping of chemically distinct domains at well-defined organic interfaces using frictional force microscopy. *J. Phys. Chem.* 99:10960–10965.

Hähner, G., A. Marti, and N. D. Spencer. 1997. The influence of pH on friction between oxide surfaces in electrolytes, studied with lateral force

microscopy: application as a nanochemical imaging technique. *Tribol. Lett.* 3:359–365.

Hansma, H. G., K. J. Kim, D. E. Laney, R. A. Garcia, M. Argaman, M. J. Allen, and S. M. Parsons. 1997. Properties of biomolecules measured from atomic force microscope images: a review. *J. Struct. Biol.* 119: 99–108.

Hansma, P. K., V. B. Elings, O. Marti, and C. E. Bracker. 1988. Scanning tunneling microscopy and atomic force microscopy: application to biology and technology. *Science.* 242:209–216.

Henderson, E., C. C. Hardin, S. K. Walk, I. J. Tinoco, and E. H. Blackburn. 1987. Telomeric DNA oligonucleotides from novel intramolecular structures containing quanine-guanine base pairs. *Cell.* 51:899–908.

Hinterdorfer, P., W. Baumgartner, H. J. Gruber, K. Schilcher, and H. Schindler. 1996. Detection and localization of individual antibody-antigen recognition events by atomic force microscopy. *Proc. Natl. Acad. Sci. USA.* 93:3477–3481.

Hoh, J. H., J. P. Cleveland, C. B. Prater, J.-P. Revel, and P. K. Hansma. 1992. Quantized adhesion detected with the atomic force microscope. *J. Am. Chem. Soc.* 114:4917–4918.

Israelachvili, J. 1992. Adhesion. *In* Intermolecular and Surface Forces, 2nd Ed. Academic Press, London. 312–337.

Johnson, K. L., K. Kendall, and A. D. Roberts. 1971. Surface energy and contact of elastic solids. *Proc. R. Soc. Lond. A.* 324:301–313.

Knapp, H. F., W. Wiegräbe, M. Heim, R. Eschrich, and R. Guckenberger. 1995. Atomic force microscope measurements and manipulation of Langmuir-Blodgett films with modified tips. *Biophys. J.* 69:708–715.

Lee, G. U., L. A. Chrisey, and R. J. Colton. 1994a. Direct measurement of the forces between complementary strands of DNA. *Science.* 266: 771–773.

Lee, G. U., D. A. Kidwell, and R. J. Colton. 1994b. Sensing discrete streptavidin-biotin interactions with atomic force microscopy. *Langmuir.* 10:354–357.

Li, Y. Q., N. J. Tao, J. Pan, A. A. Garcia, and S. M. Lindsay. 1993. Direct measurement of interaction forces between colloidal particles using the scanning force microscope. *Langmuir.* 9:637–641.

Liu, Y., T. Wu, and D. F. Evans. 1994. Lateral force microscopy study on the shear properties of self-assembled monolayers of dialkylammonium surfactant on mica. *Langmuir.* 10:2241–2245.

Mate, C. M., G. M. McClelland, R. Erlandsson, and S. Chiang. 1987. Atomic-scale friction of a tungsten tip on a graphite surface. *Phys. Rev. Lett.* 59:1942–1945.

Mazzola, L. T., and S. P. A. Fodor. 1995. Imaging biomolecule arrays by atomic force microscopy. *Biophys. J.* 68:1653–1660.

McGall, G. H., A. D. Barone, M. Diggelmann, S. P. A. Fodor, E. Gentalen, and N. Ngo. 1997. The efficiency of light-directed synthesis of DNA arrays on glass substrates. *J. Am. Chem. Soc.* 119:5081–5090.

Nakagawa, T., K. Ogawa, T. Kurumizawa, and S. Ozaki. 1993. Discriminating molecular length of chemically adsorbed molecules using an atomic force microscope having a tip covered with sensor molecules. *Jpn. J. Appl. Phys.* 32:294–296.

Neumeister, J. M., and W. A. Ducker. 1994. Lateral, normal, and longitudinal spring constants of atomic force microscopy cantilevers. *Rev. Sci. Instrum.* 65:2527–2531.

Noy, A., C. D. Frisbie, L. F. Rozsnyai, M. S. Wrighton, and C. M. Lieber. 1995. Chemical force microscopy: exploiting chemically-modified tips to quantify adhesion, friction, and functional group distributions in molecular assemblies. *J. Am. Chem. Soc.* 117:7943–7951.

Noy, A., D. V. Vezenov, and C. M. Lieber. 1997. Chemical force microscopy. *Annu. Rev. Mater. Sci.* 27:381–421.

Orosz, J. M., and J. G. Wetmur. 1977. DNA melting temperatures and renaturation rates in concentrated alkylammonium salt solutions. *Biopolymers.* 16:1183–1199.

Overney, R. M., E. Meyer, J. Frommer, D. Brodbeck, R. Lüthi, L. Howald, H.-J. Güntherodt, M. Fujihira, H. Takano, and Y. Gotoh. 1992. Friction measurements on phase-separated thin films with a modified atomic force microscope. *Nature.* 359:133–135.

Overney, R. M., E. Meyer, J. Frommer, H.-J. Güntherodt, M. Fujihira, H. Takano, and Y. Gotoh. 1994. Force microscopy study of friction and elastic compliance of phase-separated organic thin films. *Langmuir.* 10:1281–1286.

Pease, A. C., D. Solas, E. J. Sullivan, M. T. Cronin, C. P. Holmes, and S. P. A. Fodor. 1994. Light-generated oligonucleotide arrays for rapid DNA sequence analysis. *Proc. Natl. Acad. Sci. USA.* 91:5022–5026.

Perry, R. H. 1992. Physical and chemical data. *In* Perry's Chemical Engineers' Handbook, 6th Ed. D. W. Green and J. O. Maloney, editors. McGraw-Hill, New York. 8–63.

Pollock, H. M. 1992. Surface forces and adhesion. *In* Fundamentals of Friction: Macroscopic and Microscopic Processes. NATO ASI Series, E. I. L. Singer and H. M. Pollock, editors. Kluwer Academic Publishers, Dordrecht, The Netherlands. 25–34.

Rabinovich, Y. I., and R.-H. Yoon. 1994. Use of atomic force microscope for the measurements of hydrophobic forces between silanated silica plate and glass sphere. *Langmuir.* 10:1903–1909.

Ruan, J.-A., and B. Bhushan. 1994. Atomic-scale friction measurements using friction force microscopy. Part I. General principles and new measurement techniques. *J. Tribol.* 116:378–388.

Saenger, W. 1988. Principles of Nucleic Acid Structure. Springer-Verlag, New York.

Savkoor, A. R. 1992. Models of friction based on contact and fracture mechanics. *In* Fundamentals of Friction: Macroscopic and Microscopic Processes. NATO ASI Series, E. I. L. Singer and H. M. Pollock, editors. Kluwer Academic Publishers, Dordrecht, The Netherlands. 111–113.

Singer, I. L. 1992. Solid lubrication processes. *In* Fundamentals of Friction: Macroscopic and Microscopic Processes. NATO ASI Series, E. I. L. Singer and H. M. Pollock, editors. Kluwer Academic Publishers, Dordrecht, The Netherlands. 237–261.

Stuart, J. K., and V. Hlady. 1995. Effects of discrete protein-surface interactions in scanning force microscopy adhesion force measurements. *Langmuir.* 11:1368–1374.

Thomas, R. C., J. E. Houston, R. M. Crooks, T. Kim, and T. A. Michalske. 1995. Probing adhesion forces at the molecular scale. *J. Am. Chem. Soc.* 117:3830–3834.

van der Vegte, E. W., and G. Hadziioannou. 1997. Scanning force microscopy with chemical specificity: an extensive study of chemically specific tip-surface interactions and the chemical imaging of surface functional groups. *Langmuir.* 13:4357–4368.

Wang, D. G., J. Fan, C. Siao, A. Berno, P. Young, R. Sapolsky, G. Ghanour, N. Perkins, E. Winchester, J. Spencer, L. Kruglyak, L. Stein, L. Hsie, T. Topaloglou, E. Hubbell, E. Robinson, M. Mittmann, M. Morris, N. Shen, D. Kilburn, J. Rioux, C. Nusbaum, S. Rozen, T. Hudson, R. Lipshutz, M. Chee, and E. Lander. Large-scale identification, mapping, and genotyping of single-nucleotide polymorphisms in the human genome. 1998. *Science*. 280:1077–1082.

Warmack, R. J., X.-Y. Zheng, T. Thundat, and D. P. Allison. 1994. Friction effects in the deflection of atomic force microscope cantilevers. *Rev. Sci. Instrum.* 65:394–399.

Weisenhorn, A. L., P. Maivald, H.-J. Butt, and P. K. Hansma. 1992. Measuring adhesion, attraction, and repulsion between surfaces in liquids with an atomic force microscope. *Phys. Rev. B.* 45:11226–11232.

Wilbur, J. L., H. A. Biebuyck, J. C. MacDonald, and G. M. Whitesides. 1995. Scanning force microscopies can image patterned self-assembled monolayers. *Langmuir.* 11:825–831.

Yang, G., J. P. Vesenka, and C. J. Bustamante. 1996. Effects of tip-sample forces and humidity on the imaging of DNA with a scanning force microscope. *Scanning.* 18:344–350.